Electronic Supplementary Material (ESI) for Materials Horizons.
This journal is © The Royal Society of Chemistry 2023

Supporting Information

Ultrathin Hierarchical Hydrogel-Carbon Nanocomposite for Highly-Stretchable Fast-Response Water-Proof Wearable Humidity Sensor

Bingqi Pan, Peipei Su, Minghui Jin, Xiaocheng Huang, Zhengbo Wang, Ruhao Zhang, He Xu, Wenna Liu, and Yumin Ye*

Department of Materials Science and Engineering, Faculty of Materials Science and Chemical Engineering, Ningbo University, Ningbo 315211, P. R. China

Corresponding author's email address: yeyumin@nbu.edu.cn

This material includes

Content ratio calculation of the pVE-3 coating based on XPS spectra.

Content ratio and crosslinking degree (CD%) calculation of different pVE coatings based on FTIR spectra.

Effect of prestrain on wrinkle structure of nanocomposite.

Fig. S1 SEM image of pVE/CS/PDMS-50% nanocomposite with the pVE coating thickness of ~800 nm.

Fig. S2 BET surface area of pVE/PDMS and pVE/CS/PDMS nanocomposites with different prestrains.

Fig. S3 Experimental setup for humidity sensing test.

Fig. S4 Current response and response/recovery time of the pVE/PDMS and pVE/CS/PDMS composite sensors.

Fig. S5 Dynamic response-recovery curve of pVE/CS/PDMS-150% sensor in the RH range of 11%-96%.

Fig. S6 Humidity hysteresis characteristic of the pVE/CS/PDMS-150% humidity sensor under bending and stretching.

Fig. S7 Stress-strain curves of the pVE/CS/PDMS-150% humidity sensors.

Fig. S8 Current variation of the pVE/CS/PDMS-150% humidity sensor after scratching up to 15 times on the surface of the nanocomposite using a pair of tweezers.

Fig. S9 SEM images of the spandex fabric before and after iCVD coating.

Table S1. Deposition conditions of homopolymer pEGDA and pVP, and their copolymer films.

Table S2. Binding energy and peak areal ratio of different carbon environments of the pVE3 films coated on CS/PDMS.

References S1-S6

Movie S1. The water-proof performance of the sensor.

Content ratio calculation of the pVE-3 coating based on XPS spectra.

The different carbon environment peaks in the C 1s high-resolution spectrum of the pVE3 film were decoupled using XPS PEAK41 software (Table S2). Among them, -C*=O- and -C*-N- are from the VP moiety, and -O-C*=O- and -C*-O- are from the EGDA moiety in the copolymer. The content ratio of VP (n_{VP}) to EGDA (n_{EGDA}) can thus be calculated using Equation (1)：

$$\frac{n_{VP}}{n_{EGDA}} = \frac{2A_{-C*=O-}}{A_{-O-C*=O-}} \quad (1)$$

where $A_{\text{-C*=O-}}$ and $A_{\text{-O-C*=O-}}$ are denoted as the percentage area of -C*=O- and -O-C*=O- peaks, respectively. A factor of 2 was introduced because each EGDA unit has two C=O bonds.[1]

Content ratio and crosslinking degree calculation of different pVE coatings based on FTIR spectra.

The ratio of VP to EGDA content and crosslinking degree in copolymers were calculated using the method previously reported in the literature.[2-4] The FTIR spectra of pEGDA, pVP, and pVE films were normalized prior to analysis. The C=O stretching peak from VP moiety at 1665 cm^{-1} and the C=O stretching peak from EGDA moiety at 1733 cm^{-1} were decoupled and the respective peak areas were obtained using OMNIC software. Assuming that the absorption coefficient of C=O stretching in VP and EGDA moieties are the same in homopolymer and copolymer, the correlation between molar concentration of VP in the copolymer (C_{VP}) and the molar concentration of VP in the homopolymer (C^*_{VP}) can be expressed by Equation (2):

$$\frac{C_{VP}}{A_{(C=O,VP)}} = \frac{C^*_{VP}}{A^*_{(C=O,VP)}} \tag{2}$$

where $A_{(C=O,\ VP)}$ and $A^*_{(C=O,\ VP)}$ represent the C=O stretching peak area of VP moiety in copolymer and homopolymer, respectively. Similarly, the molar concentration of EGDA in copolymer (C_{EGDA}) and the molar concentration of EGDA in homopolymer (C^*_{EGDA}) can be expressed by Equation (3):

$$\frac{C_{EGDA}}{A_{(C=O,EGDA)}} = \frac{C^*_{EGDA}}{A^*_{(C=O,EGDA)}} \tag{3}$$

where $A_{(C=O,\ EGDA)}$ and $A^*_{(C=O,\ EGDA)}$ represent the C=O stretching peak area of EGDA moiety in copolymer and homopolymer, respectively. Assuming that the film densities of pVP and pEGDA are the same, the ratio of VP to EGDA content can be obtained:

$$\frac{n_{VP}}{n_{EGDA}} = \frac{C_{VP}}{C_{EGDA}} = \frac{C^*_{VP}A_{(C=O,VP)}/A^*_{(C=O,VP)}}{0.5C^*_{EGDA}A_{(C=O,EGDA)}/A^*_{(C=O,EGDA)}} = \frac{2M^*_{EGDA}A_{(C=O,VP)}A_{(C=}}{M^*_{VP}A_{(C=O,EGDA)}A_{(C=}} \tag{4}$$

where M^*_{VP} and M^*_{EGDA} are the molecular weights of EGDA and VP units, respectively. A factor of 2 was introduced because each EGDA unit has two C=O bonds. The crosslinking degree (CD%) was calculated as the mole fraction of crosslinked monomer

units and can be expressed by Equation (5):

$$CD\% = \frac{2}{\frac{n_{VP}}{n_{EGDA}} + 2} * 100\% \quad (5)$$

Effect of prestrain on wrinkle structure of nanocomposite.

Periodic surface wrinkle patterns occur when films composing both relatively stiff and soft layers are under lateral compression. The compression force is related to the prestrain of the PDMS in this case. From literature, structure of the formed wrinkles are affected by the prestrain, and the wavelength (λ) and amplitude (A) of the wrinkles can be calculated using Equation (6) and (7):[5]

$$\lambda = \frac{2\pi t(\bar{E}f/3\bar{E}s)}{1+\varepsilon_{pre}} \tag{6}$$

$$A = \frac{t\sqrt{\varepsilon_{pre}/\varepsilon_c - 1}}{\sqrt{1+\varepsilon_{pre}}} \tag{7}$$

where t is the thickness of the wrinkled film, $\bar{E}f$ and $\bar{E}s$ are the plane strain modulus of the film (pVE) and substrate (PDMS), respectively, ε_{pre} is the prestrain, and ε_c is the critical buckling strain. From Equations (6), with the increase of prestrain, the wavelength decreases, and the wrinkles become more compact. The observed morphology from SEM agrees well with this trend. From Equation (7), when the prestrain does not exceed the critical buckling strain, i.e., the value of the stress that causes the minimum deformation of the coating, the coating does not produce amplitude. The amplitude increases monotonically with respect to the prestrain when it is above the critical buckling strain, which can be deduced from calculating the partial derivatives and is also in accordance with literature.[6]

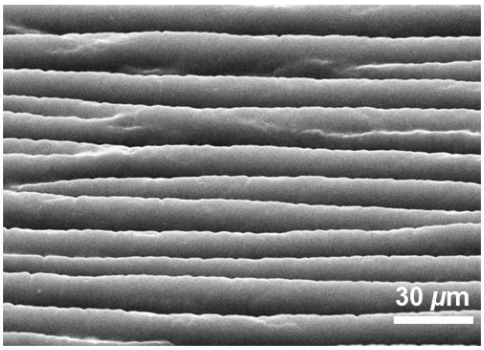

Fig. S1 SEM image of pVE/CS/PDMS-50% nanocomposite with the pVE coating thickness of ~800 nm.

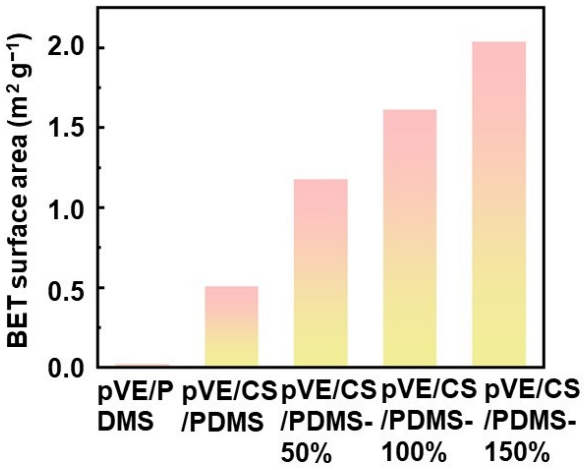

Fig. S2 BET surface area of pVE/PDMS and pVE/CS/PDMS nanocomposites with different prestrains.

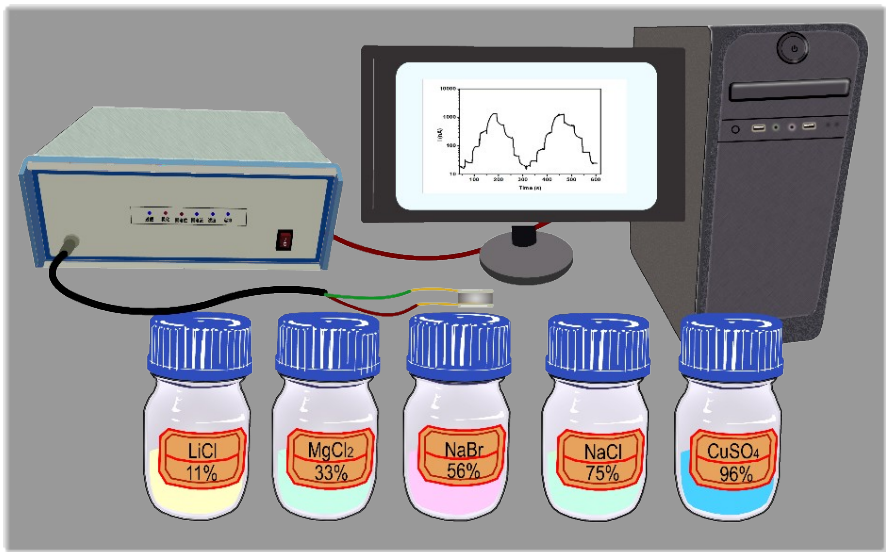

Fig. S3 Experimental setup for humidity sensing test.

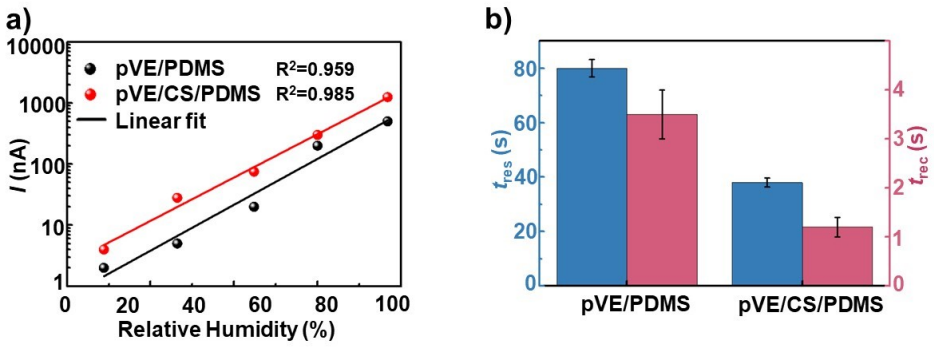

Fig. S4 a) Fitting of the response current of sensors made from pVE/PDMS and pVE/CS/PDMS nanocomposite versus RH. b) Response/recovery time of the pVE/PDMS and pVE/CS/PDMS composite sensors.

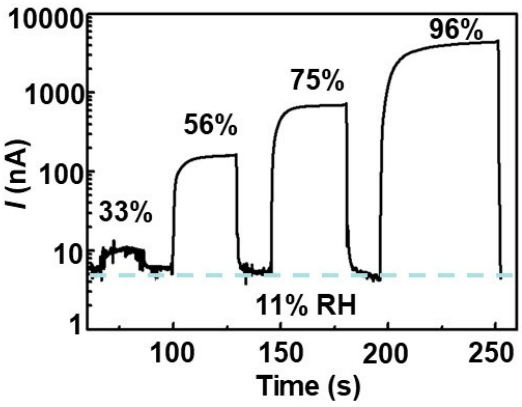

Fig. S5 Dynamic response-recovery curve of pVE/CS/PDMS-150% sensor in the RH range of 11%-96%.

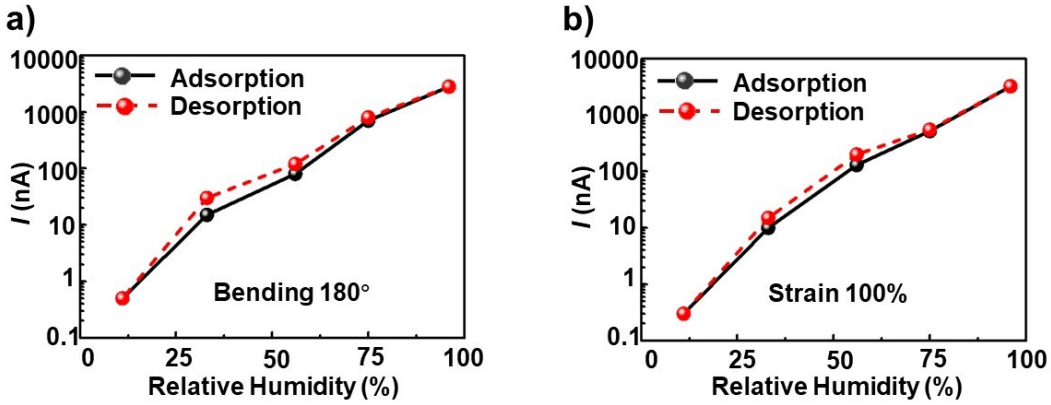

Fig. S6 Humidity hysteresis characteristic of the pVE/CS/PDMS-150% humidity sensor under a) bending at 180° and b) stretching at 100%.

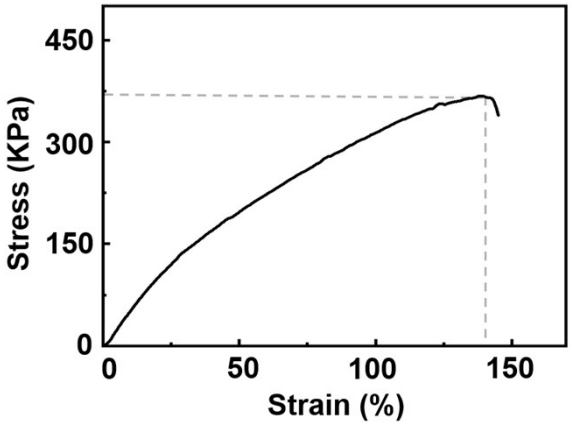

Fig. S7 Stress-strain curve of the pVE/CS/PDMS-150% humidity sensor.

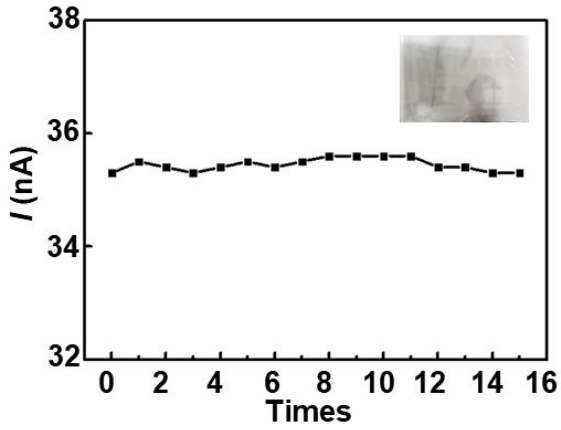

Fig. S8 Current variation of the pVE/CS/PDMS-150% humidity sensor after scratching up to 15 times on the surface of the nanocomposite using a pair of tweezers.

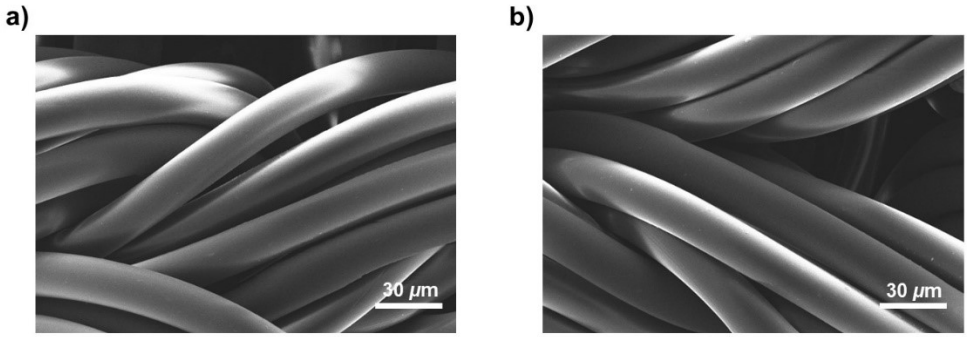

Fig. S9 SEM images of the spandex fabric a) before and b) after iCVD coating.

Table S1. Deposition conditions of homopolymer pEGDA and pVP, and copolymer p(VP-*co*-EGDA), and the content ratio of VP to EGDA and crosslinking degree in the resultant

Sample	Flow rate (sccm)			Pressure (mTorr)	Thickness (nm)	n_{VP}/n_{EGDA}	CD (%)
	TBP	EGDA	VP				
pEGDA	0.60	0.08	/	300	400	/	/
pVE-1	0.60	0.06	1.26	300	400	4	33.3
pVE-2	0.60	0.04	1.85	300	400	6	25.0
pVE-3	0.60	0.04	2.38	300	400	10	16.7
pVP	0.60	/	0.72	300	400	/	/

Table S2. Binding energy and peak areal ratio of different carbon environments of the pVE3 films coated on CS/PDMS.

Peak	Carbon environment	Binding energy (eV)	Areal ratio (%)
1	—C*—C—	284.8	52.9
2	—C*—(C=O)—	285.4	11.5
3	—C*—N—	286.1	21.0
4	—C*—O—	286.9	2.0
5	—C*=O—	287.9	10.5
6	—O—C*=O—	288.8	2.1

References

(S1) M. Sun, H. Qiu, C. Su, X. Shi, Z. Wang, Y. Ye and Y. Zhu, *ACS Appl. Bio Mater.*, 2019, **2**, 3983-3991.

(S2) Y. Ye and Y. Mao, *J. Mater. Chem.*, 2011, **21**, 7946-7952.

(S3) X. Shi, Y. Ye, H. Wang, F. Liu and Z. Wang, *ACS Appl. Mater. Interfaces*, 2018, **10**, 38449-38458.

(S4) Y. Ye, Q. Song and Y. Mao, *J. Mater. Chem.*, 2011, **21**, 257-262.

(S5) J. Yin, J. L. Yaguee, D. Eggenspieler, K. K. Gleason and M. C. Boyce, *Adv. Mater.*, 2012, **24**, 5441-5446.

(S6) R. N. Enright and L. C. Bradley, *Adv. Funct. Mater.*, 2022, **32**, 2204887.